5664–5677 *Nucleic Acids Research, 2018, Vol. 46, No. 11* *Published online 10 May 2018*
doi: 10.1093/nar/gky326

APE1 deficiency promotes cellular senescence and premature aging features

Mengxia Li[1,*,†], Xiao Yang[1,†], Xianfeng Lu[1], Nan Dai[1], Shiheng Zhang[1], Yi Cheng[1], Lei Zhang[1], Yuxin Yang[1], Yie Liu[2], Zhenzhou Yang[1], Dong Wang[1,*] and David M. Wilson, III[2,*]

[1]Cancer Center of Daping Hospital, Third Military Medical University, No. 10 Changjiang Zhi Rd., Yuzhong Dist., Chongqing 400042 China and [2]Laboratory of Molecular Gerontology, National Institute on Aging, Intramural Research Program, National Institutes of Health, 251 Bayview Blvd., Ste. 100, Baltimore, MD 21224, USA

Received November 13, 2017; Revised April 10, 2018; Editorial Decision April 11, 2018; Accepted April 23, 2018

ABSTRACT

Base excision repair (BER) handles many forms of endogenous DNA damage, and apurinic/apyrimidinic endonuclease 1 (APE1) is central to this process. Deletion of both alleles of *APE1* (a.k.a. *Apex1*) in mice leads to embryonic lethality, and deficiency in cells can promote cell death. Unlike most other BER proteins, APE1 expression is inversely correlated with cellular senescence in primary human fibroblasts. Depletion of APE1 via shRNA induced senescence in normal human BJ fibroblasts, a phenotype that was not seen in counterpart cells expressing telomerase. APE1 knock-down in primary fibroblasts resulted in global DNA damage accumulation, and the induction of $p16^{INK4a}$ and $p21^{WAF1}$ stress response pathways; the DNA damage response, as assessed by γ-H2AX, was particularly pronounced at telomeres. Conditional knock-out of *Apex1* in mice at post-natal day 7/12 resulted in impaired growth, reduced organ size, and increased cellular senescence. The effect of *Apex1* deletion at post-natal week 6 was less obvious, other than cellular senescence, until ∼8-months of age, when premature aging characteristics, such as hair loss and impaired wound healing, were seen. Low APE1 expression in patient cancer tissue also correlated with increased senescence. Our results point to a key role for APE1 in regulating cellular senescence and aging features, with telomere status apparently affecting the outcome.

INTRODUCTION

Cellular senescence is an irreversible cell cycle arrest that can be initiated by various endogenous or exogenous factors, such as replication-induced telomere shortening, genotoxin exposure, or high expression of certain oncogenes. Cellular senescence plays a role in several critical physiological processes, such as development, tumor inhibition and promotion, tissue repair, and aging (1,2). Hallmarks of senescent cells include irreversible growth arrest, enlarged morphology, increased activity of senescence-associated β-galactosidase (SA-β-gal), high levels of $p16^{INK4a}$ and/or $p21^{WAF1}$, and a senescence-associated secretary phenotype (SASP) (3,4). Mechanistically, at least two major tumor suppressor signaling pathways are involved in the initiation of senescence: $p16^{INK4a}$/pRB and $p21^{WAF1}$/p53, both of which can be triggered by a persistent DNA damage response (DDR), highlighting the importance of DNA damage and repair in the process (5). Notably, the accumulation of DNA damage has been widely implicated in premature aging, neurodegeneration and other diseases (6,7).

DNA base or sugar damage is one of the most common forms of genetic alteration, likely contributing to the genomic instability observed during aging and in disease. Base excision repair (BER) is a major pathway for removing oxidative or alkylative DNA lesions, playing a central role in preserving genome integrity, particularly under conditions of oxidative stress. BER is commonly initiated by one of a collection of lesion-specific DNA glycosylases, which recognize a substrate base and cleave the N-glycosylic bond to generate an apurinic/apyrimidinic (AP or abasic) site product. The abasic site is then typically processed by an AP endonuclease (APE1), which creates a single-strand break with a 3′-hydroxyl priming group and a 5′-abasic fragment. The resulting gap is filled and the 5′-terminus polished by DNA polymerase β (POLB), prior to ligation by nuclear DNA ligase 3α, which is mostly in complex with x-ray cross-

*To whom correspondence should be addressed. Tel: +1 410 558 8153; Email: wilsonda@mail.nih.gov
Correspondence may also be addressed to Dong Wang. Tel: +86 23 68757151; Email; dongwang64@hotmail.com
Correspondence may also be addressed to Mengxia Li III. Tel: +86 23 68757158; Email: mengxia.li@outlook.com
†The authors wish it to be known that, in their opinion, the first two authors should be regarded as Joint First Authors.

complementing protein 1 (XRCC1) (reviewed in (8)). The biological importance of BER is underscored by the fact that deletion of the core BER enzymes leads to embryonic lethality in mice (9,10).

It has been reported that BER proteins levels, as well as their enzymatic activities and response to target lesions, undergo age-associated changes (reviewed in (11)). These changes have been shown to alter the repair kinetics and lead to the accumulation of BER substrates or intermediates, such as abasic sites, in human fibroblasts and leukocytes from old donors (12). Although the phenomenon of age-associated BER alterations has been extensively studied, the participation of BER enzymes in the process of cellular senescence remains mostly uncharacterized.

Previous studies have looked at correlations of APE1, a core enzyme in the BER pathway and a transcriptional modulator via its redox regulatory function (13), with the development of senescence in various cell types. Heo *et al*. reported reduced APE1 levels in human mesenchymal stem cells that underwent senescence, with overexpression of APE1 correcting this phenotype (14). APE1 downregulation was also observed in embryonic stem cells that had senesced (15). Moreover, high APE1 expression has been reported in breast cancer tumor-initiating cells, potentially protecting these cells from irradiation-induced oxidative stress and consequent senescence (16). Intriguingly, APE1, but not POLB or XRCC1, was shown to impart this protective effect, implying a specialized role for APE1 in regulating cellular senescence. Though APE1 has long been postulated to be a critical player in cellular senescence, there have been no causal studies examining the role of the protein in this process. In the current study, we investigated the contribution of APE1 in mitigating cellular senescence in several cultured fibroblast models, a novel APE1 knock-out mouse model and human clinical samples.

MATERIALS AND METHODS

Cell culture

BJ, BJ-5ta, GM05565 and GM00969 primary human fibroblasts were obtained from American Type Culture Collection (Manassas, VA, USA). Cells were cultured in Dulbecco's modified Eagle's medium (HyClone Laboratories, Logan, UT, USA) supplemented with 10% FBS (HyClone Laboratories, Logan, UT), and were grown under normal conditions in a 9.5% CO_2 atmosphere at 37°C.

Animal husbandry and treatment

Apex1$^{flox/flox}$Cre-ER^{+} (Apex1$^{-/-}$) mice were established at the Model Animal Research Center of Nanjing University, China (see Results). The mice were kept in a temperature-controlled (22–25°C) environment with a 12-h light/dark cycle in the Animal Centre of Daping Hospital, Third Military Medical University and had free access to food and water. All experimental protocols were approved by the Research Committee of the Third Military Medical University. Tamoxifen was introduced by intraperitoneal injection to induce *Apex1* gene deletion in two schedules: (a) mice [Apex1$^{-/-}$ and Apex1$^{+/+}$Cre-ER^{+} (Apex1$^{+/+}$); unless otherwise specified] were injected with tamoxifen (10 mg/ml in corn oil with 10% ethanol) at post-natal day 7 and 12, and specified end-points were measured at ∼1 month; or (b) mice (see above) were injected with tamoxifen (30 mg/ml in corn oil with 10% ethanol) for five consecutive days at ∼6–8 weeks after post-natal development, and phenotypes were evaluated up to ∼10 months. PCR genotyping was performed to determine the *Apex1* exon 3 and Cre status following tamoxifen treatment. Animal phenotypes were evaluated by visual inspection every ∼2 days after completing the tamoxifen injection in regards to overall size, skin and hair integrity, feeding habits and other abnormal behaviors. *Apex1* knock-out efficiency was verified by western blot analysis after animals were sacrificed. For analysis of fresh tissue, different organs were isolated after heart perfusion with phosphate-buffered saline (PBS), whereas for fixed tissue, heart perfusion was performed with 4% paraformaldehyde. Fresh tissues were immediately processed by frozen sectioning or protein extraction using liquid nitrogen grounding and stored at −80°C. Fixed organs were further fixed by soaking in 4% paraformaldehyde at 4°C overnight, followed by automated tissue sectioning (Leica, Wetzlar, Germany) in the pathology department. Hematoxylin-eosin (HE) staining of tissue sections with a thickness of 2 μm was carried out using an automated staining system (Leica, Wetzlar, Germany). For immunohistochemistry, tissue sections with a thickness of 3–5 μm were used. For wound healing, several different wounds, including a simple knife incision or a round skin lesion, were introduced on the back of mice with different genotypes immediately after depilation. Regular observation of the wound healing process was performed every day up to 15 days post-incision. Wound healing and hair loss were assessed by the naked eye (and photographed), and confirmed by HE staining of skin lesion samples.

APE1 shRNA knock-down

Lentiviral particles loaded with APE1 shRNAs were packaged by co-transfection of the specific pLKO shuttle vector (clone numbers: TRCN0000007959 and TRCN0000007961, Sigma, St. Louis, MO, USA) with pCMV-VSV-G and pCMV-dR8.2 dvpr (Adgene, Cambridge, MA, USA) into 293T cells using XtremGENE HP transfection reagents (Roche, Indianapolis, IN) according to the protocol of (17). For APE1 knock-down experiments, packaged lentiviral particles were infected into human fibroblasts at the indicated passage number under selection with 2.5 μg/ml puromycin (Sigma, St. Louis, MO). After 48–72 h, cells were harvested for protein expression level determination or phenotype measurements.

DNA damage quantification

The level of AP sites was determined using the DNA Damage Quantification Kit (Dojindo, Kumamoto, Japan). In brief, genomic DNA was isolated and purified using the Genomic DNA Mini Kit (Invitrogen, Carlsbad, CA, USA). The DNA solution (100 μg) was mixed with the ARP Solution and incubated for 1 h at 37°C, prior to purifying the ARP-labelled DNA with a filtration tube. The ARP-DNA was then diluted and mixed with DNA Binding Solution

before being incubated in a 96-well plate at room temperature overnight and subsequently processed according to the manufacturer's specifications. The O.D. of each well was measured at 650 nm, and the number of abasic sites in the sample was determined using a calibration curve.

To evaluate the level of general genome DNA damage, long-range PCR was performed with Expand™ Long Template PCR System (Roche, Indianapolis, IN, USA) as previously described (18). PCR of a 17.7-kb fragment located in the 5′ flanking region near the beta-globin gene (GenBank Accession Number J00179) was conducted with the following primers: 5′-TTGAGACGCATGAGACGTGCAG-3′ and 5′-GCACTGGCTTAGGAGTTGGACT-3′. PCR conditions were as follows: denaturation for 1 min at 94°C, followed by 16 cycles of 94°C for 15 s and 68°C (primer extension) for 10 min. An additional 8 cycles were then performed as above, except 15 s were added to each cycle. A final extension was performed at 72°C for 10 min at the completion of the PCR profile. To ensure quantitative conditions, a control reaction containing half the amount of DNA template was included. The DNA concentration of each PCR product was measured using the PicoGreen assay (Life Technologies, Waltham, MA, USA) according to manufacturer's protocol.

Telomeric PCR to detect replication-blocking lesions, such as abasic sites, was performed as previously described (19) with minor modifications. Genomic DNA was isolated as above, and quantitative telomeric PCR was run on a MiniOpticon™ system (Bio-Rad, Hercules, CA, USA). In brief, a master mix [i.e., 10 μl Power SYBR Green master mix (2×), 1 μl primer telomere-fwd (CGGTTTGTTTGG GTTTGGGTTTGGGTTTGGGTTTGGGTT, 2 μM), 1 μl primer telomere-rev (GGCTTGCCTTACCCTTACCC TTACCCTTACCCTTACCCT, 2 μM) and 4 μl H_2O] was prepared, mixed and briefly centrifuged. Next, 400 ng of genomic DNA was pipetted into each well of the PCR plate. The plate was then sealed with optical clear film, centrifuged briefly and stored at 4°C. Cycling conditions were: 10 min at 95°C, followed by 40 cycles of 95°C for 15 s, 60°C for 1 min, followed by a dissociation curve. Values were exported in csv format, and used to calculate the relative amplification in the scramble and shAPE1 cells.

Protein extracts and western blot analysis

To prepare whole-cell extracts, cells or animal tissues were homogenized in extraction buffer (50 mM Tris–HCl, 0.1% sodium dodecylsulfate [SDS], 150 mM NaCl, 100 μg/ml phenylmethylsulfonyl fluoride, 1 μg/ml aprotinin, 1% nonidet P-40, and 0.5% sodium orthovanadate), incubated at 4°C for 20 min and centrifuged for 10 min at 10 500 × g. The protein levels in the extracts were quantified using the DC protein assay (Bio-Rad, Hercules, CA). For western blotting, whole-cell extracts (20 μg/lane) were resolved on 8–15% SDS-polyacrylamide gel and transferred to a nitrocellulose membrane (0.45 μm; Millipore, Bedford, MA, USA) in 25 mM Tris-base, 190 mM glycine and 20% methanol using a semidry blotter. Membranes were blocked with 10% fat-free milk and 0.1% Tween 20 in Tris-buffered saline for 1 hr, and then incubated with a primary antibody (with milk as above or 5% bovine serum albumin for the phospho-specific antibodies): APE1 (ab137708, Abcam, Cambridge, MA, USA), XRCC1 (ab134056, Abcam, Cambridge, MA), POLB (ab26343, Abcam, Cambridge, MA), OGG1 (ab124741, Abcam, Cambridge, MA), NTH1 (ab191413, Abcam, Cambridge, MA), $p16^{INK4A}$ (Clone G175-1239, BD Bioscience, San Jose, CA, USA), $p21^{WAF1}$ (ab107099, Abcam, Cambridge, MA), γ-H2AX (clone JBW301, Millipore, Billerica, MA, USA), pS1981-ATM (cat# EP1890Y, Epitomics, Cambridge, MA), pS2056-DNA-PKcs (ab18192, Abcam, Cambridge, MA) and 53BP1 (Cat# EPR2172, Epitomics, Cambridge, MA). The membranes were then incubated with an appropriate horseradish peroxidase (HRP)-conjugated secondary antibody (1:5000) (Pierce, Rockford, IL, USA). The proteins were detected using an enhanced chemiluminescence detection system (Pierce, Rockford, IL), and light emission was captured on X-ray films (Kodak, Rochester, NY, USA).

Flow cytometry

Cell apoptosis was measured using an Annexin V-fluorescein isothiocyanate/propidium iodide staining kit (BD Bioscience, San Jose, CA, USA) via flow cytometry. In brief, cells were plated in 96-well plates, incubated overnight, and then divided into the control or test group. After 24 hr of treatment, cells were harvested and washed with PBS. The cell suspensions were then double-stained with 50 μl of propidium iodide and 50 μl of Annexin V-fluorescein isothiocyanate for 15 min at room temperature while avoiding light. Apoptotic cells were determined by flow cytometry in the Third Military Medical University flow cytometry facility, and 10 000 events were recorded for the analysis.

Immunofluorescence

Cells were grown on chamber slides, allowed to attach, and fixed in 4% paraformaldehyde–PBS (w/v) at room temperature for 15 min. Cells were permeabilized with 0.1% Triton X-100 in PBS (PBST) for 5 min, and then blocked with 1% BSA at room temperature for 1 hr, followed by overnight incubation with a primary antibody against TRF2 (Cat# NB100-56506, Novus Biologicals, Littleton, CO, USA), γH2AX (clone JBW301, Millipore, Billerica, MA) or 53BP1 (Cat# 8296-1, Epitomics, Cambridge, MA) at 4°C in a humidity chamber. Cells were washed the next day with PBST on a rocking board for 15 min, and then incubated with secondary antibodies (1:200 dilution) for 1 hr at room temperature. Slides were washed again with PBST, and counterstained with DAPI for 5 min to identify the nucleus. Cells were mounted with anti-fade mounting medium, images were captured using a LSCM (laser scanning confocal microscope, Leica SP5, Germany), and image processing was performed using the LAS X software (Leica AG, Germany).

Immunofluorescence-fluorescence *in situ* hybridization (FISH)

Cells were grown on a coverslip, fixed in 4% paraformaldehyde for 10 min at room temperature, then incubated in

0.5% Triton X-100 at room temperature for 30 min. The coverslip was subsequently washed and incubated in blocking solution for 1 hr at room temperature. Cells were incubated with primary antibody (rabbit polyclonal γ-H2AX, 1:400 dilution; CST, Danvers, MA, USA) in blocking solution at room temperature for 1 hr, then washed with blocking solution and incubated with blocking solution containing DyLight 488 conjugated secondary antibody for 1 hr at room temperature. The coverslip was again washed, incubated in 4% paraformaldehyde for 10 min, washed in ethanol series solutions, denatured at 85°C for 3–5 min, hybridized with the PNA probe (Cy3-labelled CCCTAA; Panagene, Korea) overnight at 37°C, washed and mounted with DAPI stain, and finally visualized using confocal microscopy (Jena, Germany).

Tissue immunohistochemistry

Immunohistochemistry for the BER proteins was conducted using the same antibodies as used during western blotting (see above); a separate antibody was used to detect the cell proliferating marker Ki-67 (Ca# ab16667, Abcam, Cambridge, MA). In brief, sections from paraffin-embedded tissues were incubated with the indicated primary antibody overnight at 4°C and then rinsed with PBS and incubated with its associated HRP-conjugated secondary antibody for 30 min at room temperature. Sections were rinsed with PBS and developed with diaminobenzidine substrate, and then counterstained with haematoxylin for nuclear staining. Positive staining was detected as a brown color. A random 10 high power fields or at least 1,000 tumor cells were counted, and the expression of the target protein was evaluated based on the following criteria: negative (−): brown staining in <10% of the cell population; positive (+): brown staining in ≥10% of the cell population; positive (++): brown staining in ≥30% of the cell population; positive (+++): brown staining in ≥60% of the cell population. Scoring was performed by two experienced pathologists independently, and any discrepancies were resolved by a third pathologist to reach a final classification. Negative (−) and positive (+) were defined as low expression, while positive (++) and (+++) were defined as high expression.

SA-β-gal staining

β-Galactosidase activity was detected by using the Senescence Cells Histochemical Staining Kit (Sigma, St. Louis, MO). In brief, cells or frozen tissue sections were washed twice with PBS. The wash solution was removed, and 2 ml of Fixation Buffer was added and incubated with the samples for 5 min at room temperature. Cells or tissue sections were washed twice with PBS, and 1 ml of the Staining Mixture was added overnight at 37°C (without CO_2), when the cells or tissues were then stained blue. Samples were sealed with parafilm to prevent drying out. Blue-stained cells were then quantified relative to total cells, and percentage senescence was determined. Based on analysis of 1000 tumor cells from at least 10 random high-power fields, SA-β-gal staining was classified as either negative (−): blue–green staining in <10% of the cell population or positive (+): blue–green staining in ≥10% of the cell population.

Telomere restriction fragment analysis

Genomic DNA extracted from BJ cells was digested with HinfI and RsaI for 10–15 min in a 37°C water bath. Digested genomic DNA was then separated in an 0.8% agarose gel at 40 V for 20 hr and subsequently transferred to a nitrocellulose membrane using standard Southern blotting. Following overnight transfer, DNA was fixed to the membrane by UV irradiation and then incubated with a ^{32}P[dCTP] labelled [TTAGGG]n telomere probe at 42°C for at least 4 hr. Visualization was carried out on a Typhoon FLA PhosphorImager (GE Healthcare Bio-Sciences Pittsburgh, PA). The average telomere length was determined in comparison to the molecular weight standard using ImageQuant™ TL software (GE Healthcare Bio-Sciences Pittsburgh, PA, USA).

Statistical analysis

All data were expressed as the mean ± standard deviation. Statistical analysis of data was assessed using the Student's *t*-test and one-way ANOVA with the software SPSS 13.0. Differences with $P < 0.05$ were considered statistically significant for both *in vivo* and *in vitro* experiments. Correlation analysis between various BER protein levels and SA-β-gal staining in cancer tissue was performed by Spearman's rank correlation test, and $P < 0.05$ was considered statistically significant.

RESULTS

Senescence of primary human fibroblasts results in altered expression of BER proteins

To investigate a potential role of BER in the process of senescence, we employed an *in vitro* model that involves prolonged cultivation of primary human fibroblasts (20). As a means of verifying the model, we stained cells for SA-β-gal, a biomarker of senescence (representative images are shown at passage 3 (P3), P30 and P50 in Figure 1A). Expectedly, with an increase in passage number, we observed an increase in the percentage of primary BJ fibroblasts that stained positive for SA-β-gal (Figure 1B). Using this model, we measured the levels of individual BER proteins at early, mid and late passages—i.e. P3, P30 and P50, respectively—by western blot analysis. These studies revealed that APE1 and endonuclease three homolog 1 (NTH1) are reproducibly downregulated during the process of senescence, whereas the level of XRCC1 significantly increased. POLB and 8-oxoguanine DNA glycosylase 1 (OGG1) remained largely unchanged during the extended culturing, based on three independent replicates (Figure 1C and D).

Using the same methodology on hTERT (telomerase reverse transcriptase)-immortalized BJ fibroblasts (BJ-5ta), we found that SA-β-gal staining remained low during continuous culturing *in vitro* (Supplementary Figure S1A and B), consistent with prior evidence that hTERT expression can suppress the development of senescence (21). Moreover, all BER proteins remained stably expressed (or slightly increased in the case of APE1) during culturing, indicating that hTERT-mediated suppression of senescence preserves normal BER protein expression in normal fibroblasts (Supplementary Figure S1C and D). Collectively, our cell culture

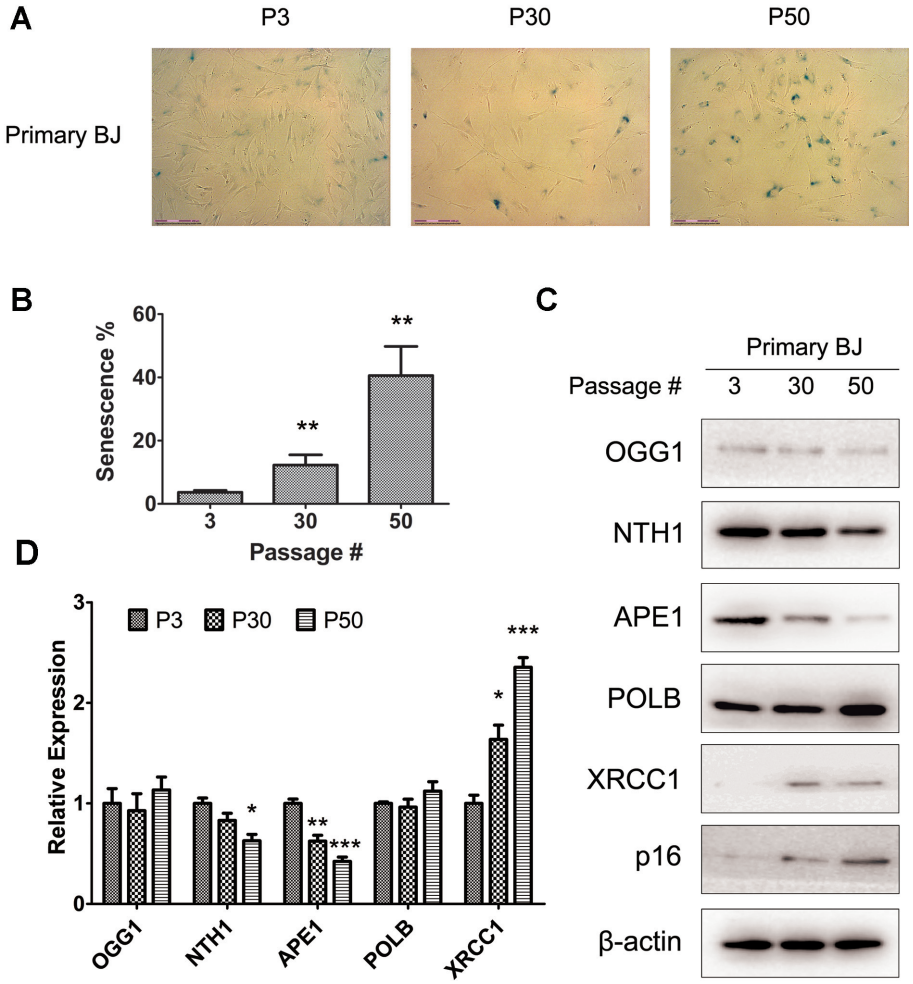

Figure 1. Senescence results in altered expression of BER proteins in primary human BJ fibroblasts. (**A**) Representative images of SA-β-gal staining at P3, P30 and P50 in primary BJ fibroblasts. (**B**) Quantitation of the percentage of cells that has undergone senescence (SA-β-gal positive) at the indicated passage number. (**C**) Expression of several BER proteins at P3, P30 and P50 as determined by western blot analysis. Increased $p16^{INK4a}$ expression is consistent with a senescent phenotype. (**D**) Quantitation of expression of the indicated BER protein (after normalization to the β-actin loading control) relative to the P3 group. In panels B and D, results are averages and standard deviations of three biological replicates. **P*-value < 0.05, ***P*-value < 0.01, ****P*-value < 0.001

models indicate that BER components may participate in or be responsive to the process of cellular senescence in a way that might be determined by telomere status.

APE1 deficiency induces cellular senescence in an hTERT-influenced manner

As APE1 is downregulated during cellular senescence (Figure 1 and (14–16,22)), we examined whether knocking-down APE1 in early passage primary fibroblasts would induce senescence. Specifically, we employed two different lentiviral particles loaded with APE1 shRNAs [TRCN0000007959 (#59) and TRCN0000007961 (#61)] to deplete APE1 protein in three different normal primary fibroblasts. Through SA-β-gal staining, we found that infection of either APE1-specific lentiviral particle, but not the scramble control, resulted in an increase in the percentage of senescent cells in early passage BJ (virus infected at P2–5), GM05565 (at P3–8) and GM00969 (at P10–15) primary fibroblasts (Figure 2A and B). As clone TRCN0000007959 showed the most effective knock-down of APE1 (Figure 2C), we used this lentivirus for all subsequent APE1 depletion experiments. Additional senescence markers, including $p16^{INK4a}$ and $p21^{WAF1}$, were assayed by western blotting upon APE1 knock-down in the three primary fibroblasts. These studies found that $p16^{INK4a}$ and $p21^{WAF1}$ are elevated in APE1-deficient cells, in comparison to the scramble controls, suggesting that the $p16^{INK4a}$/pRB and $p21^{WAF1}$/p53 senescence pathways are both activated upon APE1 depletion, although the degree to which varied among the different cellular backgrounds (Figure 2C).

To more broadly assess the contribution of BER substrates in inducing senescence, we examined the effect of POLB or XRCC1 knock-down on senescence in the three normal fibroblasts. Although POLB expression did not change and XRCC1 levels actually went up during the senescence process (Figure 1C and D), we found that targeted depletion of either POLB or XRCC1 increased senescence in the three cellular backgrounds (Figure 2D and Supplementary Figure S2A). These data strongly implicate

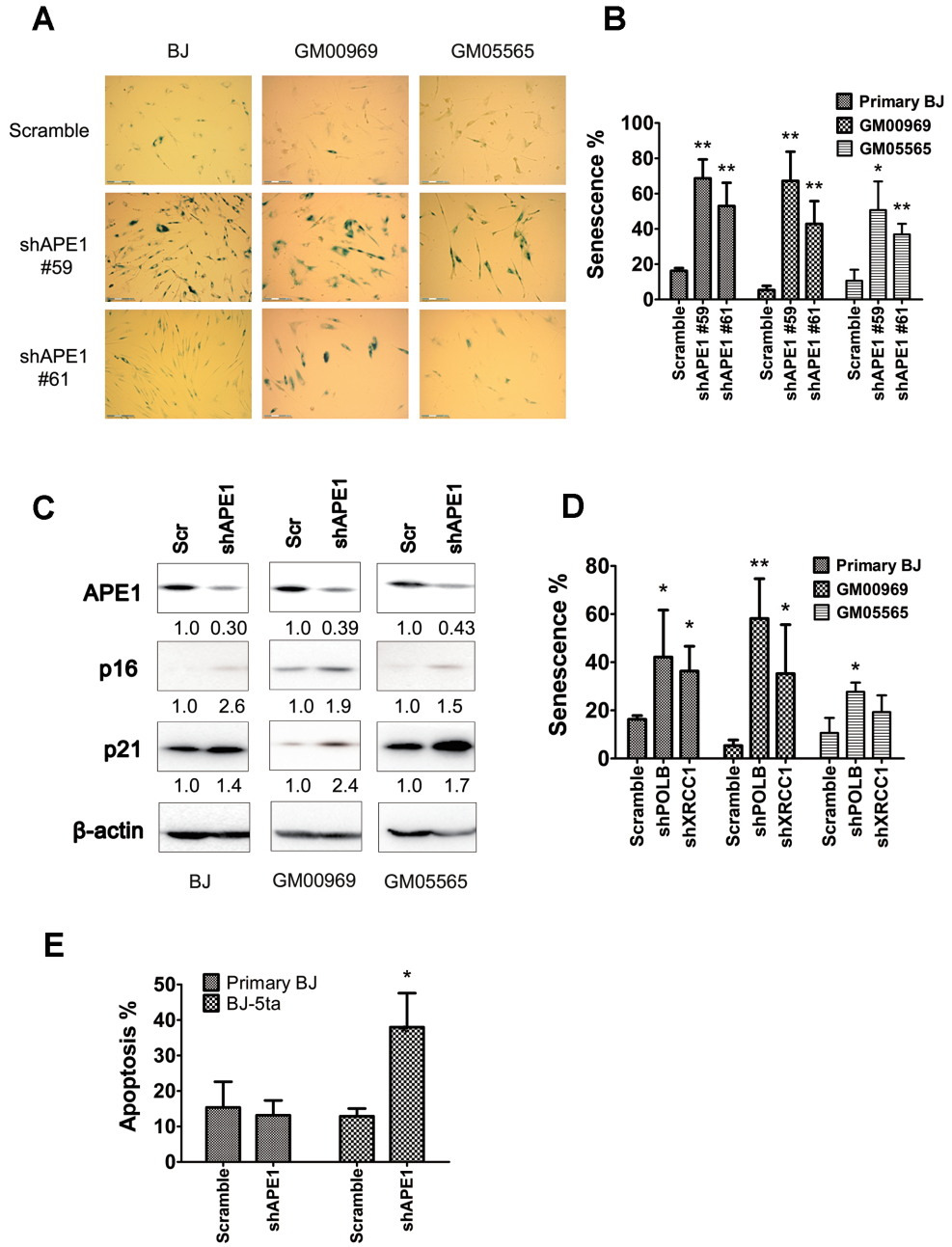

Figure 2. APE1 knock-down results in increased cellular senescence in hTERT-negative fibroblasts. (**A**) Representative images of SA-β-gal staining in BJ (at P2–5), GM05565 (at P3–8) and GM00969 (at P10–15) fibroblasts that were infected at the indicated passage number with an APE1-specific shRNA [TRCN0000007959 (#59) or TRCN0000007961 (#61)] or the scramble control. Sample analysis was conducted 48–72 hr post-infection. (**B**) Quantitation of the percentage of cells that have undergone senescence in early passage fibroblasts following APE1 knock-down or scramble control. (**C**) The expression of APE1, $p16^{INK4a}$ and $p21^{WAF1}$ in the indicated scramble control (Scr) or APE1-knock-down (shAPE1) cell population, as determined by western blot analysis. Following normalization of the indicated protein to β-actin, the relative expression level (specified below each) was obtained by comparing knock-down to its corresponding scramble control. (**D**) Quantitation of the percentage of cells that have undergone senescence (SA-β-gal) in early passage primary BJ, GM05565 and GM00969 fibroblasts upon shRNA knock-down of POLB or XRCC1. (**E**) Quantitation of the percentage of cells that have undergone apoptosis in hTERT-negative (primary BJ) or hTERT-positive (BJ-5ta) cells following APE1 knock-down (shRNA, #59), in comparison to the scramble control. Results are averages and standard deviations of three biological replicates (panel B and D) or two biological replicates with three technical replicates each (panel E). **P*-value < 0.05, ***P*-value < 0.01

BER and endogenous DNA damage as central factors in regulating this outcome. However, in the case of POLB- and XRCC1-deficient fibroblasts, while $p21^{WAF1}$ was typically elevated, $p16^{INK4a}$ remained mostly unchanged, suggesting that distinct molecular steps give rise to cellular senescence due to a defect in BER that require further investigation (Supplementary Figure S2B).

Previous studies found that defects in the core BER enzymes, including APE1, primarily resulted in apoptosis in a wide-range of cancer cell lines (e.g. HeLa cervical adenocarcinoma (23), A549 lung adenocarcinoma (24,25), SH-SY5Y neuroblastoma (26,27), T98G glioblastoma (28,29) and PC12 pheochromocytoma (30,31)), which are hTERT-positive (32). Since we observed that APE1 deficiency induced senescence in hTERT-negative BJ cells (see above), we explored the effects of APE1 knock-down in the counterpart hTERT-positive BJ-5ta fibroblasts (where APE1 expression was found to go unchanged with continuous culturing; see above). These experiments revealed that in BJ-5ta cells, APE1 deficiency markedly promoted apoptotic cell death (Figure 2E), whereas no increase in apoptosis was observed in primary BJ cells upon APE1 knock-down, implying that APE1 defects can drive distinct cellular fates, depending on hTERT expression and presumably telomere status.

APE1 deficiency promotes broad DNA damage accumulation and a telomere-driven DDR

To measure DNA damage in the general genome or the telomeric region, we used long-range PCR, which targets a 17.7-kb fragment in the 5′ flanking region near the beta-globin gene, or telomeric PCR, respectively. Both assays are sensitive to replication (PCR)-blocking lesions, such as strand breaks and AP sites. As shown in Figure 3, a reduced PCR efficiency (reflective of higher DNA damage) was observed in the general genome (∼27%, panel A) and at telomeres (∼49%, panel B) in APE1-deficient BJ fibroblasts (relative to scramble controls), indicating that loss of APE1 broadly leads to DNA damage accumulation. Using telomere restriction fragment analysis, we observed that telomere length was not significantly altered after APE1 knock-down (Figure 3C), despite the increased levels of DNA damage. We also found by western blotting that several DDR-related proteins, including phosphorylated H2A histone family, member X (γ-H2AX), phosphorylated-Ser1981 ataxia telangiectasia mutated (pATM), phosphorylated-Ser2056 DNA-dependent protein kinase, catalytic subunit (pDNA-PKcs), and tumor suppressor p53-binding protein 1 (53BP1), are generally hyperactivated in APE1-deficient primary BJ fibroblasts (Figure 3D), reflective of a broad cellular DDR. When APE1 was knocked-down in hTERT-expressing BJ-5ta cells (where apoptosis was the major outcome; Figure 2E), there was an increase in general genomic DNA damage (Supplementary Figure S3A), while telomere damage and length remained unchanged (Supplementary Figure S3B,C). In addition, APE1-deficient BJ-5ta cells exhibited specific activation of γ-H2AX and DNA-PKcs, and not pATM or 53BP1, relative to the scramble control (Supplementary Figure S3D), likely reflecting an apoptosis-initiated cleavage and activation event, a conclusion in-line with the increased apoptosis measured by flow cytometry (Figure 2E).

As previous reports showed a specific protective role of APE1 at telomeres (33), and in light of the hTERT-effects reported above, we hypothesized that APE1 knock-down might trigger a telomere-driven DDR. To test this idea, we employed an immunofluorescence-FISH assay to evaluate co-localization of the DNA damage marker γ-H2AX and telomeric DNA (Cy3-labelled CCCTAA PNA probe) in APE1-deficient BJ fibroblasts (Figure 3E). These studies revealed that there are significantly more cells harboring >5 γ-H2AX foci upon APE1 knock-down in comparison to the scramble control population (83.8% versus 12.7%, respectively; Figure 3F). In addition, a significant increase (∼3-fold) in the percentage of γ-H2AX foci that co-localize with the telomeric DNA probe was observed in APE1-deficient cells (Figure 3G). We also observed increased γ-H2AX foci co-localizing with the telomeric marker TRF2 (telomere repeat-binding factor 2) in APE1-deficient BJ fibroblasts (Supplementary Figure S4A). These collective data are consistent with γ-H2AX activation (and a consequent DDR) occurring predominantly at the telomeric region as a result of APE1 deficiency. Using a chromatin immunoprecipitation (ChIP) assay followed by dot blotting and probing with a telomeric sequence, we observed APE1 bound at telomeres (with or without hydrogen peroxide treatment; Supplementary Figure S4B), consistent with a prior report detecting APE1 at telomeric regions (33).

Apex1 knock-out causes senescence in mice

To explore the role of APE1 (a.k.a. Apex1 in mouse) in various biological and pathophysiological phenomena, we established an *Apex1* tamoxifen-inducible conditional knock-out mouse model using the process overviewed in Supplementary Figure S5. Specifically, a loxP site was inserted both upstream and downstream of exon 3 of the *Apex1* gene on chromosome 14 to eliminate protein production following the administration of tamoxifen, which promotes translocation of a transgenically-expressed Cre-ER (estrogen receptor) recombinase into the nucleus. To determine the effect of early *Apex1* knock-out (before weaning) on development and aging, the $Apex1^{flox/flox}$Cre-ER^{+} (abbreviated $Apex1^{-/-}$ hereafter) mutant and the $Apex1^{+/+}$Cre-ER^{+} (abbreviated $Apex1^{+/+}$ hereafter) control mice were injected with tamoxifen at post-natal day 7 and then again at day 12 (Figure 4A). The efficiency of gene knock-out was assessed at day 28 by measuring Apex1 protein expression in various tissues/organs from the surviving floxed ($Apex1^{-/-}$) and wild-type ($Apex1^{+/+}$) animals ($n = 4$ mice per group) via western blotting. As shown in Figure 4B, the Apex1 protein level was reduced by >95% in heart, skin, lung and pancreas in the tamoxifen-treated $Apex1^{-/-}$ animals relative to the $Apex1^{+/+}$ controls, with a trace amount of Apex1 being visible in the brain and colon of the knock-out animals at day 28. In contrast, although significantly reduced, there remained a considerable amount of Apex1 protein in the kidney, liver and spleen of the $Apex1^{-/-}$ mice. Thus, while *Apex1* knock-out is quite efficient following tamoxifen exposure, there does exist variability in the degree of *Apex1* deletion that is tissue/organ-specific in

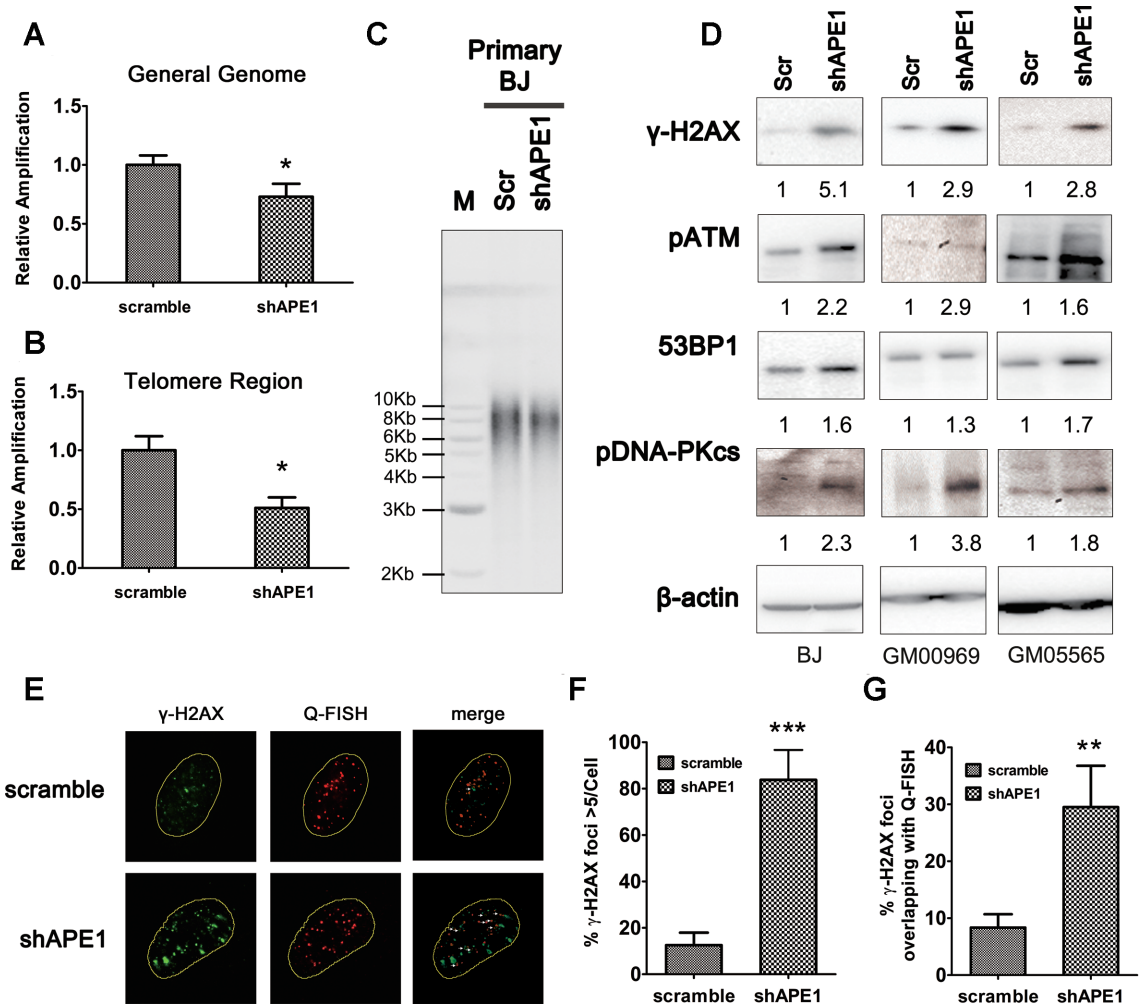

Figure 3. APE1 knock-down results in elevated genomic DNA damage and increased γ-H2AX foci at telomeres. DNA damage was quantified in the general genome (**A**) or telomeric region (**B**) of APE1-deficient (shAPE1) BJ fibroblasts relative to the scramble control using a targeted PCR strategy. See Figure 2 for general overview of experimental approach. (**C**) Telomere length was assayed by Southern blotting in scramble control (Scr) or APE1 knock-down (shAPE1) BJ fibroblasts. A representative image is shown, and the molecular standards are indicated. (**D**) Expression of γ-H2AX, pATM, 53BP1 and pDNA-PKcs was determined by western blotting in APE1-deficient (shAPE1) and scramble control (Scr) primary fibroblasts (designated). β-actin served as the loading control, and relative expression level (in comparison to relevant scramble control) is designated below each lane. (**E**) Immunofluorescence-FISH of γ-H2AX and PNA probe (Q-FISH) in APE1-deficient (shAPE1) and control (scramble) BJ fibroblasts. Nuclei are designated by yellow dashed line and white arrows indicate colocalization of the two signals. (**F**) Quantitation of the percentage of cells that exhibit >5 γ-H2AX foci/cell. (**G**) Quantitation of the percentage of overlap between γ-H2AX and telomeric DNA (Q-FISH foci). Graphical results represent averages and standard deviations of three biological replicates with at least four technical replicates each (panel A and B) or three biological replicates (panel F and G). **P*-value < 0.05, ***P*-value < 0.01, ****P*-value < 0.001.

the current model. Tissue/cell-specificity of the tamoxifen-inducible systems has been recognized for decades (see, e.g. (34)), including in the CAGGCre-ER™ animal model used here (The Jackson Laboratory; (35)), and likely stems from variability in exposure to the inducing agent and the efficiency of expression of the Cre-recombinase gene within its unique nuclear/chromosome environment.

We note that 84% (21/25) of Apex1$^{-/-}$ mice (i.e., Apex1$^{flox/flox}$Cre-ER^{+} treated with tamoxifen at days 7 and 12) died before weaning (day 28), as compared to 5% (1/20) of Apex1$^{flox/flox}$Cre-ER^{+} animals not treated with tamoxifen. The reasons for this dramatic increase in mortality following early *Apex1* deletion are under investigation, but likely stem from severe developmental and growth defects, as previously seen in the germline knock-out animals (36,37). Nevertheless, examination of the surviving Apex1$^{-/-}$ mice and the Apex1$^{+/+}$ tamoxifen-treated controls (n = 4 mice per group) revealed that the Apex1-deficient animals were dramatically smaller in size in comparison to their age-matched wildtype counterparts (Figure 4C), as were most of the organs, including the heart, digestive track, kidney, spleen and brain (Figure 4D), which were found to exhibit a range in efficiency of target gene deletion (Figure 4B). Furthermore, using SA-β-gal staining, we found that cellular senescence is significantly elevated in the skin (~100% *Apex1* gene deletion) and colon (~70% deletion), especially in epithelial cells, of Apex1$^{-/-}$ mice relative to the Apex1$^{+/+}$ controls (Figure 4E). Furthermore, we found no difference in TUNEL staining in these two organs of Apex1$^{+/+}$ or Apex1$^{-/-}$ mice, indicating that apoptosis

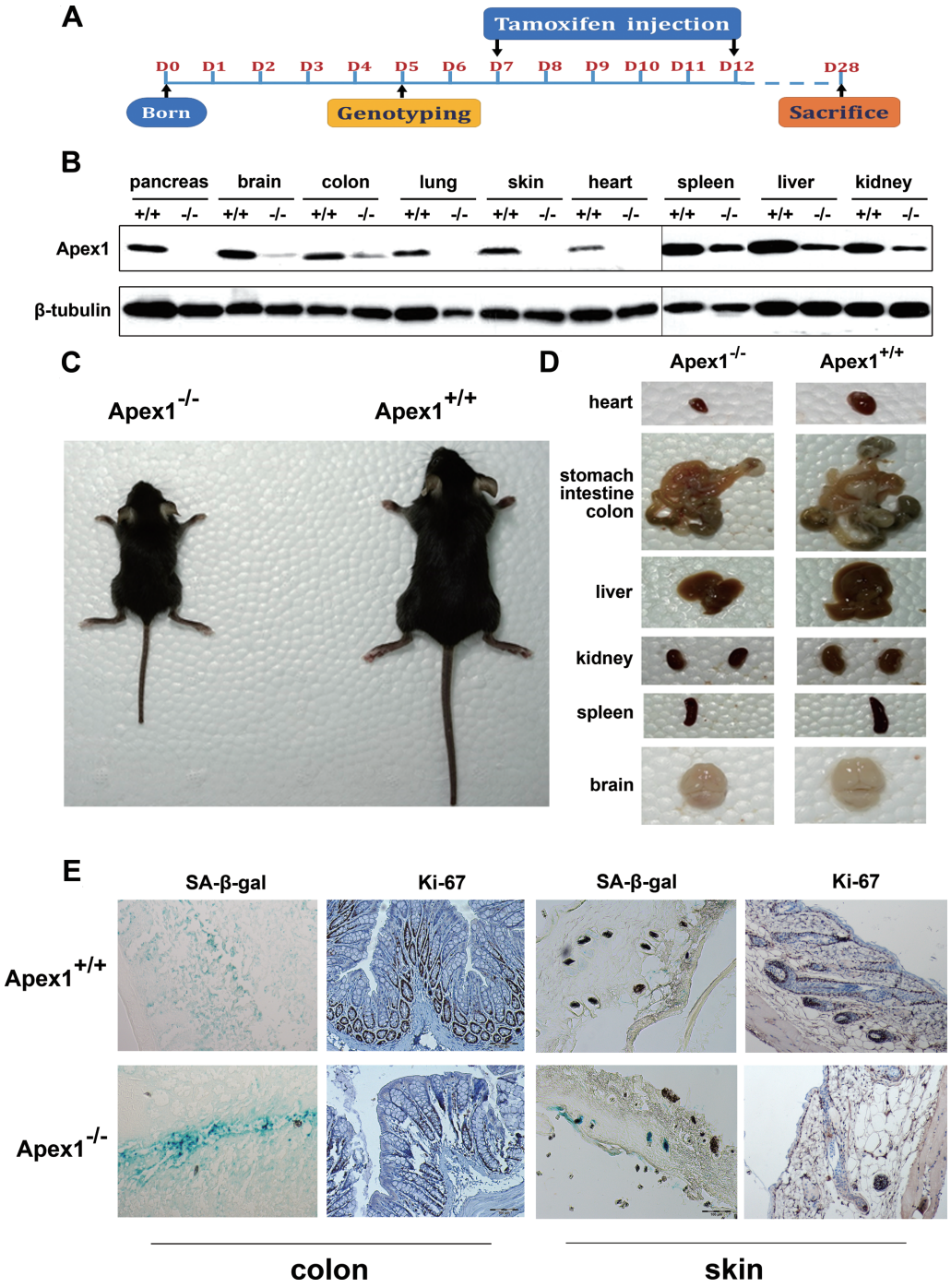

Figure 4. Effect of *Apex1* deletion at post-natal day 7/12 on mouse growth and organ development. (**A**) Tamoxifen treatment strategy for post-natal day 7/12 (D7/D12) mice. (**B**) Expression of Apex1 protein in the indicated tissue/organ of tamoxifen-treated wildtype ($Apex1^{+/+}$) or Apex1-floxed ($Apex1^{-/-}$) animals ($n = 4$ mice per group). Shown is a representative western blot using Apex1 or β-tubulin (loading control) antibody. (**C**) Comparison of overall size of $Apex1^{-/-}$ and $Apex1^{+/+}$ animals ($n = 4$ mice per group) at D28. (**D**) Comparison of tissues/organs, including heart, digestive track, liver, kidney, spleen and brain of $Apex1^{-/-}$ and $Apex1^{+/+}$ animals ($n = 4$ mice per group) after sacrifice at D28. (E) SA-β-gal staining and immunohistochemistry for Ki67 in the colon and skin of $Apex1^{-/-}$ and $Apex1^{+/+}$ mice ($n = 4$ mice per group).

was not obviously affected by reduced Apex1 protein levels (Supplementary Figure S6A,B). These data cumulatively are consistent with our earlier observations using normal human fibroblasts, and support the concept that APE1 deficiency can lead to a senescent phenotype.

We next examined whether gene knock-out at week 6 (post-weaning, by injecting tamoxifen for five consecutive days; Figure 5A) had a noticeable long-term pathophysiological consequence. As shown in Figure 5B, at 10-months of age, the Apex1 protein expression pattern among the various organs was essentially identical to that of the early knock-out cohort (compare with Figure 4B). However, in the situation here (i.e. tamoxifen treatment at week 6), the phenotypic differences between Apex1$^{-/-}$ and Apex1$^{+/+}$ mice ($n = 6$ animals per group) were quite subtle, until at least 8-months of age. In contrast to the early *Apex1* knock-out cohort (Figure 4D), there were no significant differences in organ sizes between the two experimental groups at 10-months of age, except for the larger spleen seen in the Apex1$^{-/-}$ mice (Figure 5C), possibly due to immunosuppression after *Apex1* deletion. Nevertheless, Apex1$^{-/-}$ mice ($n = 6$) displayed notable hair loss (Figure 5D) and exhibited impaired skin wound healing (Figure 5E), attributes often associated with aging.

In light of the premature aging features, we examined cellular senescence in the skin and colon (again, organs with slight differences in *Apex1* gene deletion efficiency) of mutant (Apex1$^{-/-}$) and control (Apex1$^{+/+}$) animals treated with tamoxifen at week 6, employing SA-β-gal staining, as well as an immunohistochemistry assay for Ki-67, a cellular marker for proliferation. Although SA-β-gal staining can be spotted in Apex1$^{+/+}$ mice, it is significantly higher in the epithelial cells of Apex1$^{-/-}$ samples ($n = 6$ mice per group) (Figure 5F and G). The DDR marker, γ-H2AX, as well as p16^{INK4a} and p21^{WAF1}, are all increased significantly in the Apex1$^{-/-}$ group (assayed by western blot, Figure 5H and I), again consistent with the findings for APE1-deficient human fibroblasts. Indeed, we observed elevated p16^{INK4a} and p21^{WAF1} in the skin and colon of greater than 20 Apex1$^{-/-}$ animals in comparison to Apex1$^{+/+}$ tamoxifen-treated controls (unpublished observation). Since the major DNA damage substrate of APE1 is the abasic site, we quantified this lesion using an aldehyde-reactive probe (ARP) assay (Figure 5J). These experiments found that AP sites increased ∼2-fold in the skin and colon of Apex1$^{-/-}$ mice in comparison to control animals. Collectively, our studies indicate that DNA damage, such as abasic lesions, accumulates in Apex1-deficient animals, leading to the activation of a DDR and ultimately cellular senescence, as well as developmental or pathological consequences that are influenced by the timing of gene deletion. However, it is important to emphasize that our analysis does not clearly identify which function of APE1 (e.g. repair endonuclease or redox regulation) is responsible for suppressing senescence.

Low APE1 protein level is associated with senescence in clinical samples

Given that APE1 deficiency leads to senescence in both human cell and mouse models, we examined relevant clinical material for this correlative outcome. First, we established 10 primary fibroblast cultures from excess skin removed during plastic surgery. We then used the TRCN0000007959 lentiviral system to knock-down APE1 in these fibroblasts at passage 3–5 and measured senescence via the SA-β-gal assay relative to the scramble control (Figure 6A). These studies, collectively plotted in Figure 6B, further support that knock-down of APE1 in primary fibroblasts induces cellular senescence.

Second, we assayed BER protein expression by immunohistochemistry and senescence by SA-β-gal staining in cancer tissue from 22 patients with breast, thyroid or glioblastoma malignancies (Supplementary Figure S7). We then 'quantified' the expression of NTH1, OGG1, APE1, POLB or XRCC1 as a degree of positive staining [i.e. 3 = high (+++), 2 = medium high (++), 1 = medium low (+), or 0 = low or negative (−); see Materials and Methods], and visually presented these expression results with respect to positive or negative SA-β-gal staining (Figure 6C). Notably, we found that low staining for APE1, but not the other BER proteins (or age), was associated with higher levels of tissue senescence ($r^2 = –0.432$, $P = 0.045$; Supplementary Table S1), further supporting a role for APE1 in mitigating this biological outcome.

DISCUSSION

The free radical theory of aging proposes that the gradual accumulation of oxidative damage plays a role in the deterioration of cellular function and the aging phenomenon. BER, which has a prominent responsibility in repairing oxidative DNA damage, has long been considered a major protective mechanism against cellular senescence, a biological outcome associated with aging. In our current study, we show for the first time a causative relationship between deficiency in APE1, an essential BER enzyme, and the emergence of cellular senescence, *in vitro*, *in vivo* and in clinical samples.

We observed that the APE1 protein level, unlike several other BER proteins, was significantly reduced in a manner that correlated with the extent of senescence in hTERT-negative primary human fibroblasts during prolonged culturing. We subsequently found that APE1 knock-down induced cellular senescence in multiple primary skin fibroblast sources. Notably, previous studies have reported that defects in the core BER enzymes, including APE1, mainly result in apoptosis in a wide-range of cancer cell lines, which are commonly hTERT-positive (as mentioned in the Results section, see (23–32)). Since we observed that APE1 deficiency induced senescence in hTERT-negative BJ cells, yet promoted apoptosis in the counterpart hTERT-positive BJ cells, we speculate that APE1 deficiency drives two distinct cellular fates dependent on hTERT expression and presumably telomere status.

Previous work has demonstrated that APE1 deficiency results in telomere dysfunction, illustrated by significant and persistent γ-H2AX foci formation at telomeres, in human U2OS osteosarcoma epithelial cells, a line that harbors an activated alternative lengthening of telomeres (ALT) pathway, as well as in BJ-hTERT fibroblasts and HeLa cells, which express hTERT (33). We observed the same telomeric accumulation of γ-H2AX foci in primary human fibrob-

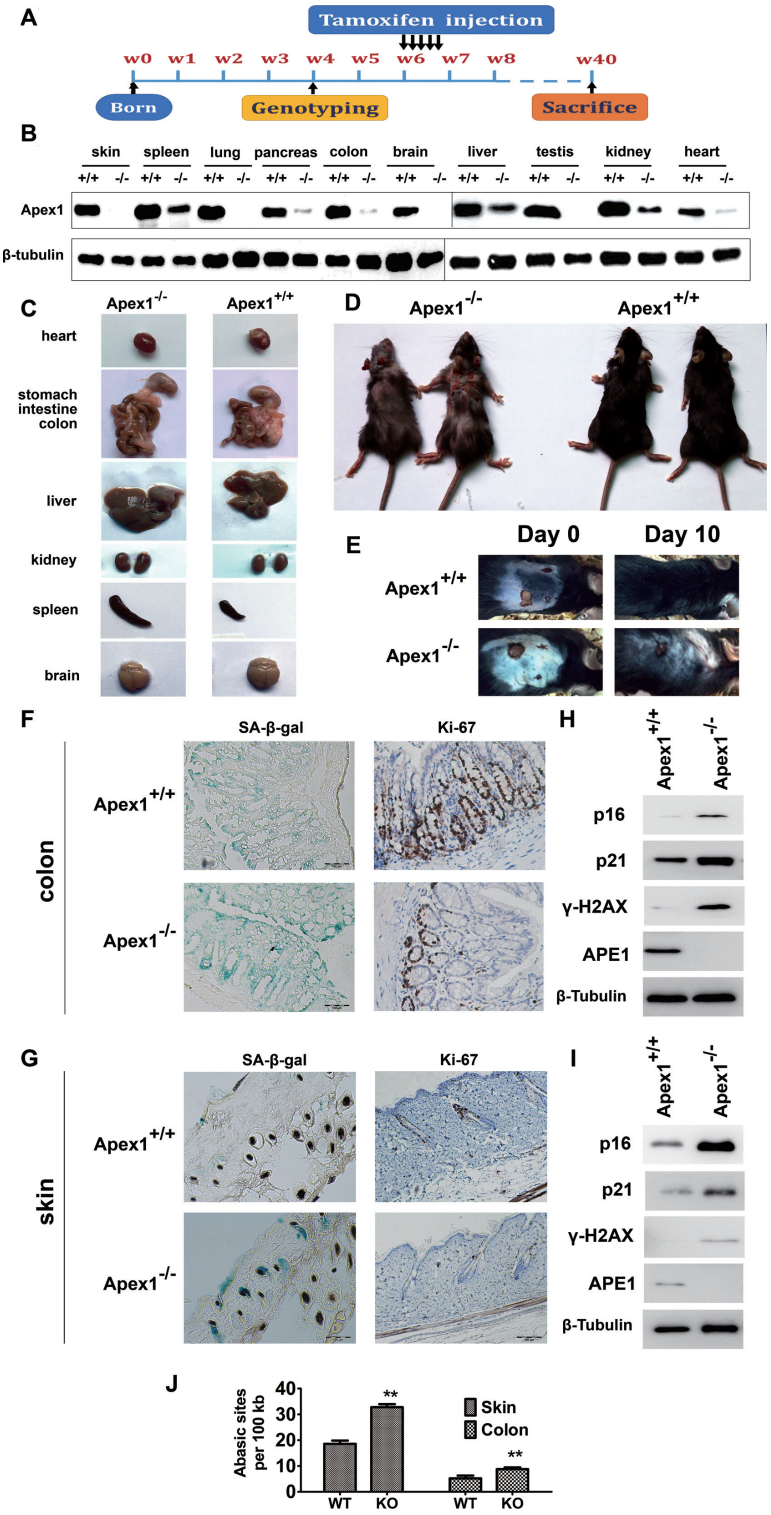

Figure 5. Effect of *Apex1* deletion at post-weaning week 6 on animal health. (**A**) The protocol for tamoxifen treatment of post-weaning week 6 (W6) mice. (**B**) Expression of Apex1 protein in the indicated tissue/organ of tamoxifen-treated wild-type ($Apex1^{+/+}$) or Apex1-floxed ($Apex1^{-/-}$) animals ($n =$ 6 mice per group). Shown is a representative western blot using Apex1 or β-tubulin (loading control) antibody. (**C**) Comparison of the tissues/organs of $Apex1^{-/-}$ and $Apex1^{+/+}$ mice ($n = 6$ mice per group). (**D**) Comparison of the overall size of the $Apex1^{-/-}$ and $Apex1^{+/+}$ animals ($n = 6$ mice per group). Analysis of animals and associated tissue/organs was carried out at W40. (**E**) Comparison of skin wound healing after incision of the back of $Apex1^{+/+}$ and $Apex1^{-/-}$ animals ($n = 6$ mice per group). Representative images of wound at day 0 and 10 days post-incision are shown. SA-β-gal staining and Ki67 immunohistochemistry in the colon (**F**) and skin (**G**) of $Apex1^{-/-}$ and $Apex1^{+/+}$ mice (n = 6 mice per group). The expression of $p16^{INK4a}$, $p21^{WAF1}$, γ-H2AX and Apex1 was determined in extracts from the colon (**H**) or skin (**I**) of $Apex1^{-/-}$ and $Apex1^{+/+}$ mice ($n = 6$ mice per group) by western blot analysis. (**J**) The amount of abasic sites in skin and colon of $Apex1^{-/-}$ and $Apex1^{+/+}$ animals ($n = 6$ mice per group). Results are the average and standard deviation of three biological replicates with four technical replicates each. $^{**}P$-value < 0.01.

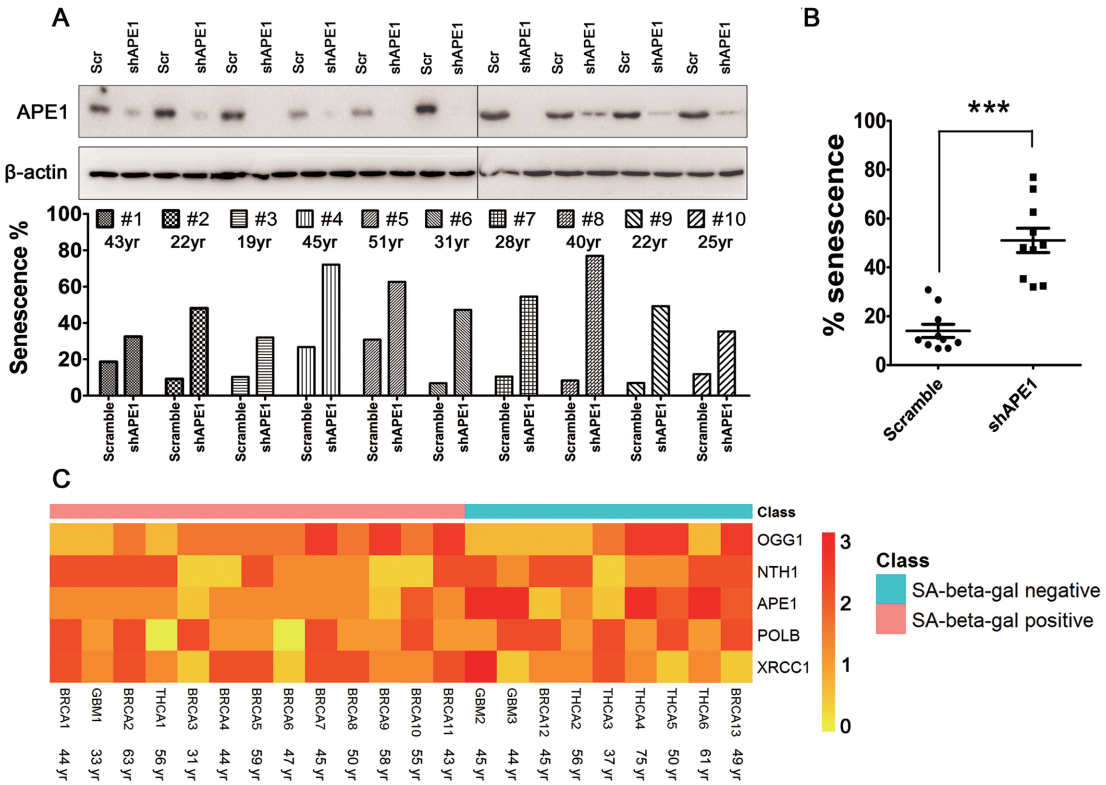

Figure 6. BER protein expression correlates with senescence in patient samples. (**A**) Knock-down of APE1 (shAPE1; #59) in 10 primary fibroblast cultures from the excess skin removed during plastic surgery results in increased senescence relative to the scramble control. Results from a single run of each human fibroblast culture is shown below the relevant sample. (**B**) The results (% senescence, i.e. SA-β-gal positive) from each sample in panel A are plotted for the scramble control and comparative APE1 knock-down cells. Averages and standard deviations are indicated, with ***P-value < 0.001. (**C**) Heat map of BER protein expression in cancerous tissue of all surveyed patients as measured by immunohistochemistry. 3 (dark red) = high, 0 (yellow) = low or negative expression. BER proteins and SA-β-gal classification (negative or positive) are designated. Patients (including age) are defined below, with breast cancer indicated by 'BRCA', glioblastoma indicated by 'GBM', and thyroid cancer indicated by 'THCA'.

lasts, suggesting that APE1 has a critical role in telomere DNA protection in many different cell types. In addition, we detected increased levels of two important senescent markers, $p16^{INK4a}$ and $p21^{WAF1}$, following APE1 knock-down or knock-out, indicating that telomere-dependent and/or DDR-induced senescence signaling pathways are activated in APE1-deficient cells.

We found that APE1 depletion resulted in the accumulation of replication-blocking lesions (likely abasic sites) in both telomeric and general genomic regions, yet increased the DDR foci primarily at telomeres. Thus, our data suggests that APE1 depletion triggers activation of the two major pathways of cellular senescence (reviewed in (38)), likely originating from telomeric defects. Consistent with a major repair function at telomeres, we showed previously that APE1 exhibits a proficient incision activity at abasic sites in the context of double-stranded telomeric repeats *in vitro* (39). In addition, APE1 has been demonstrated to associate with telomeric shelterin proteins, TRF2 and protection of telomeres protein 1 (POT1), which enhance its AP endonuclease activity on abasic telomeric substrates *in vitro* (40,41). As seen previously (33), we also found that APE1 binds at telomeric repeats, suggesting that APE1 routinely resides at the telomere region to facilitate efficient repair. Notably, due to their hexameric G-rich repeats and single-stranded nature, telomeres accumulate higher levels of oxidative damage than many regions in the genome (42–44).

Premature aging is observed in mice defective in pathways related to DNA damage repair, e.g. nucleotide excision repair, the DDR, and telomere or mitochondrial genome maintenance (45). Since mice that lack a core BER protein are embryonic lethal (36), it's been difficult to address the connection between BER defects and aging phenotypes. In the study here, we created a whole-body inducible conditional knock-out *Apex1* mouse model to examine the link between Apex1 deficiency and various pathophysiologies. When gene deletion was induced early after birth (at day 7/12), Apex1 deficiency resulted in increased mortality, likely driven by developmental/growth retardation (i.e. reduced animal and tissue/organ size) and elevated senescence. When *Apex1* was deleted after weaning at week 6, we observed no obvious growth defect up to 18-months without manipulation. We did, however, observe at roughly 10-months of age prominent age-related phenotypes, such as hair loss and reduced wound healing, as well as increased senescence in the colon and skin of $Apex1^{-/-}$ animals. We also note that when agitated, such as breeding under lower temperature or depilating the back, Apex1 knock-out mice displayed reduced survival or hair recovery, respectively (manuscript in preparation). Thus, combined with the previous studies of *Apex1* gene knock-out in mice (36,46–48),

the encoded protein appears to be critical for embryonic survival, post-natal development and healthy aging, yet may be less vital for adult survival in unstressed conditions.

By examining the levels of APE1 and other BER proteins in patient cancer tissue samples, we revealed a specific inverse correlation of APE1 expression with cellular senescence. Elevated APE1 has been reported to be associated with various cancer types, including lung, colorectal, breast, and glioblastoma etc., supporting an important role for APE1 in the carcinogenic process (reviewed in (13)). However, there are portions of cancer tissue that exhibit low or negative expression of APE1, and are frequently associated with good prognosis. Due to the tumor suppressive effect of cellular senescence, our findings connecting low APE1 expression with an increased senescent phenotype might explain this association. Thus, an interesting line of investigation would be to determine the role of APE1 in oncogene-induced senescence, which is directly involved in tumor suppression (49).

The discovery of SASP revealed a potential tumor promoting effect of senescent cells (50). In particular, most of the SASP-related secretion factors, including interleukins 6 and 8, matrix metalloproteinases, pro-neurogenic factors and pro-angiogenic factors, have been shown to promote the proliferation of precancerous and cancerous cells (51), enhance invasion, and induce an epithelial to mesenchymal transition in carcinoma cells (52). Interestingly, transcription of some of the SASP factors has been shown previously to be regulated by the redox function of APE1 (reviewed in (13)), which might bring complexity to the possible roles of APE1 in the crosstalk between senescence and cancer. How SASP is shaped in senescent cells induced by APE1 deficiency is currently under investigation.

SUPPLEMENTARY DATA

Supplementary Data are available at NAR Online.

ACKNOWLEDGEMENTS

We are grateful to Drs Huiming Lu, Evandro F. Fang, Peter Sykora from Laboratory of Molecular Gerontology of National Institute on Aging, National Institutes of Health for their technical support and discussion; Drs Yujun He (Mammary Surgery Department), Liang Yi (Neurosurgery Department), Chengyi Mao (Pathology department), Shiguang Cheng and Jiangdong Sui (Cancer Center Lab), Yuanyuan Wang and Yadong Yang (Dermatology Department) from Daping Hospital, Third Military Medical University for technical support; and Drs Xiaocui Li and Yong Zhao from SunYat-Sen University for technical assistance with the immunofluorescence-FISH method.

FUNDING

Intramural Research Program of the NIH; National Institute on Aging (NIA) (to D.M.W.); National Natural Science Foundation of China (NSFC) [81472803 to Z.Y.]; '1135' Talented Person Project of Daping Hospital (to D.W.). Funding for open access charge: NIA; IRP; NIH.
Conflict of interest statement. None declared.

REFERENCES

1. Campisi,J. and d'Adda di Fagagna,F. (2007) Cellular senescence: when bad things happen to good cells. *Nat. Rev. Mol. Cell. Biol.*, **8**, 729–740.
2. He,S. and Sharpless,N.E. (2017) Senescence in health and disease. *Cell*, **169**, 1000–1011.
3. Rodier,F. and Campisi,J. (2011) Four faces of cellular senescence. *J. Cell Biol.*, **192**, 547–556.
4. Kubben,N. and Misteli,T. (2017) Shared molecular and cellular mechanisms of premature ageing and ageing-associated diseases. *Nat. Rev. Mol. Cell Biol.*, **18**, 595–609.
5. Campisi,J. (2013) Aging, cellular senescence, and cancer. *Annu. Rev. Physiol.*, **75**, 685–705.
6. Coppede,F. and Migliore,L. (2010) DNA repair in premature aging disorders and neurodegeneration. *Curr. Aging Sci.*, **3**, 3–19.
7. Bielak-Zmijewska,A., Mosieniak,G. and Sikora,E. (2017) Is DNA damage indispensable for stress-induced senescence? *Mech. Ageing Dev.*, **170**, 13–21.
8. Kim,Y.J. and Wilson,D.M. 3rd (2012) Overview of base excision repair biochemistry. *Curr. Mol. Pharmacol.*, **5**, 3–13.
9. Brenerman,B.M., Illuzzi,J.L. and Wilson,D.M. 3rd (2014) Base excision repair capacity in informing healthspan. *Carcinogenesis*, **35**, 2643–2652.
10. Wilson,D.M. 3rd and Thompson,L.H. (1997) Life without DNA repair. *Proc. Natl. Acad. Sci. U.S.A.*, **94**, 12754–12757.
11. Gorbunova,V., Seluanov,A., Mao,Z. and Hine,C. (2007) Changes in DNA repair during aging. *Nucleic Acids Res.*, **35**, 7466–7474.
12. Atamna,H., Cheung,I. and Ames,B.N. (2000) A method for detecting abasic sites in living cells: age-dependent changes in base excision repair. *Proc. Natl. Acad. Sci. U.S.A.*, **97**, 686–691.
13. Li,M. and Wilson,D.M. 3rd (2014) Human apurinic/apyrimidinic endonuclease 1. *Antioxid. Redox Signal.*, **20**, 678–707.
14. Heo,J.Y., Jing,K., Song,K.S., Seo,K.S., Park,J.H., Kim,J.S., Jung,Y.J., Hur,G.M., Jo,D.Y., Kweon,G.R. *et al.* (2009) Downregulation of APE1/Ref-1 is involved in the senescence of mesenchymal stem cells. *Stem Cells*, **27**, 1455–1462.
15. Kruta,M., Balek,L., Hejnova,R., Dobsakova,Z., Eiselleova,L., Matulka,K., Barta,T., Fojtik,P., Fajkus,J., Hampl,A. *et al.* (2013) Decrease in abundance of apurinic/apyrimidinic endonuclease causes failure of base excision repair in culture-adapted human embryonic stem cells. *Stem Cells*, **31**, 693–702.
16. Karimi-Busheri,F., Rasouli-Nia,A., Mackey,J.R. and Weinfeld,M. (2010) Senescence evasion by MCF-7 human breast tumor-initiating cells. *Breast Cancer Res.: BCR*, **12**, R31.
17. Stewart,S.A., Dykxhoorn,D.M., Palliser,D., Mizuno,H., Yu,E.Y., An,D.S., Sabatini,D.M., Chen,I.S., Hahn,W.C., Sharp,P.A. *et al.* (2003) Lentivirus-delivered stable gene silencing by RNAi in primary cells. *RNA*, **9**, 493–501.
18. Li,M.X., Wang,D., Zhong,Z.Y., Xiang,D.B., Li,Z.P., Xie,J.Y., Yang,Z.Z., Jin,F. and Qing,Y. (2008) Targeting truncated APE1 in mitochondria enhances cell survival after oxidative stress. *Free Radic. Biol. Med.*, **45**, 592–601.
19. Cawthon,R.M. (2002) Telomere measurement by quantitative PCR. *Nucleic Acids Res.*, **30**, e47.
20. Bodnar,A.G., Ouellette,M., Frolkis,M., Holt,S.E., Chiu,C.P., Morin,G.B., Harley,C.B., Shay,J.W., Lichtsteiner,S. and Wright,W.E. (1998) Extension of life-span by introduction of telomerase into normal human cells. *Science*, **279**, 349–352.
21. Morales,C.P., Holt,S.E., Ouellette,M., Kaur,K.J., Yan,Y., Wilson,K.S., White,M.A., Wright,W.E. and Shay,J.W. (1999) Absence of cancer-associated changes in human fibroblasts immortalized with telomerase. *Nat. Genet.*, **21**, 115–118.
22. Intano,G.W., McMahan,C.A., McCarrey,J.R., Walter,R.B., McKenna,A.E., Matsumoto,Y., MacInnes,M.A., Chen,D.J. and Walter,C.A. (2002) Base excision repair is limited by different proteins in male germ cell nuclear extracts prepared from young and old mice. *Mol. Cell. Biol.*, **22**, 2410–2418.
23. Tamura,Y., Tao,M., Miyano-Kurosaki,N., Takai,K. and Takaku,H. (2000) Inhibition of human telomerase activity by antisense phosphorothioate oligonucleotides encapsulated with the transfection reagent, FuGENE6, in HeLa cells. *Antisense Nucleic Acid Drug Dev.*, **10**, 87–96.

24. Li,M.X., Shan,J.L., Wang,D., He,Y., Zhou,Q., Xia,L., Zeng,L.L., Li,Z.P., Wang,G. and Yang,Z.Z. (2012) Human apurinic/apyrimidinic endonuclease 1 translocalizes to mitochondria after photodynamic therapy and protects cells from apoptosis. *Cancer Sci.*, **103**, 882–888.
25. Ogretmen,B., Schady,D., Usta,J., Wood,R., Kraveka,J.M., Luberto,C., Birbes,H., Hannun,Y.A. and Obeid,L.M. (2001) Role of ceramide in mediating the inhibition of telomerase activity in A549 human lung adenocarcinoma cells. *J. Biol. Chem.*, **276**, 24901–24910.
26. Jiang,Y., Guo,C., Fishel,M.L., Wang,Z.Y., Vasko,M.R. and Kelley,M.R. (2009) Role of APE1 in differentiated neuroblastoma SH-SY5Y cells in response to oxidative stress: use of APE1 small molecule inhibitors to delineate APE1 functions. *DNA Repair*, **8**, 1273–1282.
27. Hossain,M.M., Banik,N.L. and Ray,S.K. (2012) Survivin knockdown increased anti-cancer effects of (−)-epigallocatechin-3-gallate in human malignant neuroblastoma SK-N-BE2 and SH-SY5Y cells. *Exp. Cell Res.*, **318**, 1597–1610.
28. Montaldi,A.P., Godoy,P.R. and Sakamoto-Hojo,E.T. (2015) APE1/REF-1 down-regulation enhances the cytotoxic effects of temozolomide in a resistant glioblastoma cell line. *Mutat. Res. Genet. Toxicol. Environ. Mutagen.*, **793**, 19–29.
29. Wang,T., Xue,Y., Wang,M. and Sun,Q. (2012) Silencing of the hTERT gene through RNA interference induces apoptosis via bax/bcl-2 in human glioma cells. *Oncol. Rep.*, **28**, 1153–1158.
30. Kang,B., Mu,S., Yang,Q., Guo,S., Chen,X. and Guo,H. (2017) Ape1 protects against MPP+-induced neurotoxicity through ERK1/2 signaling in PC12 cells. *Neuroreport*, **28**, 10–16.
31. Li,H., Pinto,A.R., Duan,W., Li,J., Toh,B.H. and Liu,J.P. (2005) Telomerase down-regulation does not mediate PC12 pheochromocytoma cell differentiation induced by NGF, but requires MAP kinase signalling. *J. Neurochem.*, **95**, 891–901.
32. Hahn,W.C. (2003) Role of telomeres and telomerase in the pathogenesis of human cancer. *J. Clin. Oncol.*, **21**, 2034–2043.
33. Madlener,S., Strobel,T., Vose,S., Saydam,O., Price,B.D., Demple,B. and Saydam,N. (2013) Essential role for mammalian apurinic/apyrimidinic (AP) endonuclease Ape1/Ref-1 in telomere maintenance. *Proc. Natl. Acad. Sci. U.S.A.*, **110**, 17844–17849.
34. Feil,R., Brocard,J., Mascrez,B., LeMeur,M., Metzger,D. and Chambon,P. (1996) Ligand-activated site-specific recombination in mice. *Proc. Natl. Acad. Sci. U.S.A.*, **93**, 10887–10890.
35. Hayashi,S. and McMahon,A.P. (2002) Efficient recombination in diverse tissues by a tamoxifen-inducible form of Cre: a tool for temporally regulated gene activation/inactivation in the mouse. *Dev. Biol.*, **244**, 305–318.
36. Xanthoudakis,S., Smeyne,R.J., Wallace,J.D. and Curran,T. (1996) The redox/DNA repair protein, Ref-1, is essential for early embryonic development in mice. *Proc. Natl. Acad. Sci. U.S.A.*, **93**, 8919–8923.
37. Ludwig,D.L., MacInnes,M.A., Takiguchi,Y., Purtymun,P.E., Henrie,M., Flannery,M., Meneses,J., Pedersen,R.A. and Chen,D.J. (1998) A murine AP-endonuclease gene-targeted deficiency with post-implantation embryonic progression and ionizing radiation sensitivity. *Mut. Res.*, **409**, 17–29.
38. Rossiello,F., Herbig,U., Longhese,M.P., Fumagalli,M. and d'Adda di Fagagna,F. (2014) Irreparable telomeric DNA damage and persistent DDR signalling as a shared causative mechanism of cellular senescence and ageing. *Curr. Opin. Genet. Dev.*, **26**, 89–95.
39. Li,M., Volker,J., Breslauer,K.J. and Wilson,D.M. 3rd (2014) APE1 incision activity at abasic sites in tandem repeat sequences. *J. Mol. Biol.*, **426**, 2183–2198.
40. Lee,O.H., Kim,H., He,Q., Baek,H.J., Yang,D., Chen,L.Y., Liang,J., Chae,H.K., Safari,A., Liu,D. *et al.* (2011) Genome-wide YFP fluorescence complementation screen identifies new regulators for telomere signaling in human cells. *Mol. Cell. Proteomics*, **10**, M110 001628.
41. Miller,A.S., Balakrishnan,L., Buncher,N.A., Opresko,P.L. and Bambara,R.A. (2012) Telomere proteins POT1, TRF1 and TRF2 augment long-patch base excision repair in vitro. *Cell Cycle*, **11**, 998–1007.
42. Evans,M.D. and Cooke,M.S. (2004) Factors contributing to the outcome of oxidative damage to nucleic acids. *BioEssays*, **26**, 533–542.
43. von Zglinicki,T. (2002) Oxidative stress shortens telomeres. *Trends Biochem. Sci.*, **27**, 339–344.
44. Prasad,K.N., Wu,M. and Bondy,S.C. (2017) Telomere shortening during aging: attenuation by antioxidants and anti-inflammatory agents. *Mech. Ageing Dev.*, **164**, 61–66.
45. Lombard,D.B., Chua,K.F., Mostoslavsky,R., Franco,S., Gostissa,M. and Alt,F.W. (2005) DNA repair, genome stability, and aging. *Cell*, **120**, 497–512.
46. Meira,L.B., Devaraj,S., Kisby,G.E., Burns,D.K., Daniel,R.L., Hammer,R.E., Grundy,S., Jialal,I. and Friedberg,E.C. (2001) Heterozygosity for the mouse Apex gene results in phenotypes associated with oxidative stress. *Cancer Res.*, **61**, 5552–5557.
47. Raffoul,J.J., Cabelof,D.C., Nakamura,J., Meira,L.B., Friedberg,E.C. and Heydari,A.R. (2004) Apurinic/apyrimidinic endonuclease (APE/REF-1) haploinsufficient mice display tissue-specific differences in DNA polymerase beta-dependent base excision repair. *J. Biol. Chem.*, **279**, 18425–18433.
48. Unnikrishnan,A., Raffoul,J.J., Patel,H.V., Prychitko,T.M., Anyangwe,N., Meira,L.B., Friedberg,E.C., Cabelof,D.C. and Heydari,A.R. (2009) Oxidative stress alters base excision repair pathway and increases apoptotic response in apurinic/apyrimidinic endonuclease 1/redox factor-1 haploinsufficient mice. *Free Rad. Biol. Med.*, **46**, 1488–1499.
49. Campisi,J. (2001) Cellular senescence as a tumor-suppressor mechanism. *Trends Cell Biol.*, **11**, S27–31.
50. Freund,A., Patil,C.K. and Campisi,J. (2011) p38MAPK is a novel DNA damage response-independent regulator of the senescence-associated secretory phenotype. *EMBO J.*, **30**, 1536–1548.
51. Krtolica,A., Parrinello,S., Lockett,S., Desprez,P.Y. and Campisi,J. (2001) Senescent fibroblasts promote epithelial cell growth and tumorigenesis: a link between cancer and aging. *Proc. Natl. Acad. Sci. U.S.A.*, **98**, 12072–12077.
52. Coppe,J.P., Patil,C.K., Rodier,F., Sun,Y., Munoz,D.P., Goldstein,J., Nelson,P.S., Desprez,P.Y. and Campisi,J. (2008) Senescence-associated secretory phenotypes reveal cell-nonautonomous functions of oncogenic RAS and the p53 tumor suppressor. *PLoS Biol.*, **6**, 2853–2868.